

COMBUSTION IN IMPULSIVELY INITIATED VORTEX RINGS

T. R. MEYER,¹ J. R. GORD,² V. R. KATTA,¹ W. M. ROQUEMORE,²
G. L. SWITZER,¹ AND G. J. FIECHTNER³

¹*Innovative Scientific Solutions, Inc.*

2766 Indian Ripple Road

Dayton, OH 45440-3638, USA

²*Air Force Research Laboratory*

Propulsion Directorate

Wright-Patterson Air Force Base, OH 45433-7103, USA

³*Sandia National Laboratories*

Combustion Research Facility

Livermore, CA 94551-0969, USA

Presented at the
2nd Joint Meeting of the U.S. Section of the Combustion Institute
Oakland, CA

March 25-28, 2001

Abstract

The mixing behavior of impulsively initiated vortex rings has been the subject of a number of previous investigations in non-reacting environments. In the current work, combustion in impulsively initiated vortex rings is studied experimentally using planar laser-induced fluorescence (PLIF) imaging of the hydroxyl radical (OH). Well-characterized vortex rings of fuel and air are generated at the exit of an axisymmetric nozzle by using a solenoid-driven piston to pulse a reservoir of methane fuel. Ignition is initiated at various locations downstream of the nozzle exit and at various times relative to vortex initiation, pinch-off, and propagation. A number of parameters affecting vortex propagation and mixing are also studied, including piston speed and stroke length. Results from PLIF visualizations are compared with corresponding data from non-reacting vortex rings and with numerical simulations from a time-dependent computational fluid dynamics code with chemistry.

COMBUSTION IN IMPULSIVELY INITIATED VORTEX RINGS

T. R. MEYER,¹ J. R. GORD,² V. R. KATTA,¹ W. M. ROQUEMORE,²
G. L. SWITZER,¹ AND G. J. FIECHTNER¹

¹*Innovative Scientific Solutions, Inc.*

2766 Indian Ripple Road

Dayton, OH 45440-3638, USA

²*Air Force Research Laboratory*

Propulsion Directorate

Wright-Patterson Air Force Base, OH 45433-7103, USA

1. Introduction

Due to their frequent occurrence in reacting flows of technological interest, vortex-flame interactions have received considerable attention in recent years. Renard et al.¹ provide a comprehensive review of numerical, theoretical, and experimental investigations of vortex-flame interactions and their effects on flame dynamics, extinction, ignition, mixing, baroclinic torque, and thermal diffusion. These investigations typically study the collision of a laminar flame front with a vortex or burning within the vortex itself. The current study falls into the latter category, which is useful for studying the effects of flow structure, vorticity, and curvature on flame ignition and propagation. Within this important subset are a number of studies of flame propagation along the axis of a premixed vortex ring. Early studies by McCormack and coworkers^{2,3} reported flame speeds of up to 15 m/s, with a linear dependence on vortex circulation. Ishizuka et al.⁴ also report super-laminar flame speeds along the vortex core, but propose a somewhat reduced dependence on vortex circulation. Cattolica⁵ and Cattolica and Vosen⁶ performed studies of premixed flame propagation in the wake of a vortex for a combustion-torch configuration. Ignition of lean premixed gases within a combustion chamber generated a vortex ring of unburned, premixed methane and air. The flame follows in the wake of the vortex and eventually propagates through the vortex rollers. Wilson et al.⁷ used a similar method of generating premixed vortex combustion for use in active combustion control.

In the current study, ignition and flame propagation in premixed methane-air vortex rings are investigated while varying the equivalence ratio, ignition timing, and vortex propagation velocity. This significantly extends the work of Cattolica⁵ and Cattolica and Vosen,⁶ who mostly considered the effect of exit velocity. Because ignition is initiated at various stages of vortex development, this investigation contains elements of flame propagation along the vortex axis as well as in the wake and roller structures. Results are compared with numerical simulations from a time-dependent computational fluid dynamics code with chemistry. In addition to giving useful insight into ignition and flame propagation in the field of a premixed vortex, practical insight is gained into the feasibility of a vortex-assisted ignition system for high-speed combustor applications.

2. Experimental Set-Up and Conditions

The jet-in-co-flow burner of the current study has been used in a number of previous investigations of vortex-flame interactions.^{8,9} In the current configuration, shown in Fig. 1, repeatable vortex rings of premixed methane and air were formed at the exit of a 5 mm-diameter

central nozzle using a solenoid-driven 25 mm-diameter piston at the bottom of the fuel tube. Ignition was initiated at various phases with respect to vortex formation and propagation using a pair of electrodes located near the nozzle periphery. A co-flow of air surrounded the fuel-air jet, and a shroud flow of nitrogen was used to reduce external disturbances. A steady background flow rate of 0.14 m/s was maintained for all flows when the piston was not being actuated. When acetone planar laser-induced fluorescence (PLIF) measurements were performed, the nozzle air supply was diverted into an acetone seeding system prior to premixing with methane.

PLIF of the hydroxyl radical (OH) was accomplished by exciting the $R_1(8)$ transition of the (1,0) band in the A-X system. The requisite 281.3414 nm laser sheet was generated using the frequency doubled output of a Nd:YAG pumped dye laser, and subsequent fluorescence from the A-X (1,1) and (0,0) bands was detected at right angles using a f/1.4 UV lens and an intensified charge-coupled device (ICCD) camera. The 576×384 pixel array was binned in 2×2 groups, and the imaged area was 26.5 mm wide × 40 mm high. Prior to detection by the ICCD, the OH PLIF signal was filtered using UG-11 and WG-295 colored glass filters to remove visible and laser scattered light, respectively. Acetone PLIF was accomplished using the same laser wavelength and camera system (without the UG-11 filter), eliminating any uncertainties due to misalignment and variations in signal generation. Although most acetone PLIF measurements were performed to characterize the *cold-flow* conditions, the 300 ns gate of the ICCD allowed the UG-11 filter to be removed for simultaneous OH and acetone PLIF. A timing circuit driven by a Quantum Composer, Inc. pulse generator allowed for synchronization of the laser pulse, camera gate, spark ignition, and piston actuation.

As shown in Table 1, three main parameters were varied during the experiments: spark timing, equivalence ratio, and vortex strength. The equivalence ratio was varied from 0.75 to 1.5, and the spark timing was varied from 2.5 ms to 8 ms after the piston stroke. The effect of vortex strength was studied by varying the piston stroke between 1.6 to 5 mm while keeping the rise time constant. This resulted in vortex propagation velocities ranging from 2.5 to 6.5 m/s, which for constant ratios of vortex core diameter to toroidal ring diameter, is proportional to the maximum tangential velocity in the vortex as well as the circulation.⁴ Since flame propagation is very sensitive to the location of the spark, the position of the electrodes was kept constant for all runs at 2-3 mm above the fuel-air nozzle, 3.5 mm apart, and just outside of the central jet. Thus, a flame could be initiated prior to, during, or after the vortex formation and propagation stages.

3. Numerical Model

Ignition and propagation of a premixed flame in the flow field of a vortex induced by a starting jet was investigated using a transient two-dimensional code known as UNICORN,¹⁰ which solves the time-dependent, axisymmetric Navier-Stokes equations along with the species- and energy-conservation equations. The chemical kinetics model for methane-air combustion consists of 17 species and 52 elementary reaction steps. Transport coefficients and properties were estimated using molecular dynamics, mixing rules, and polynomial curve-fits. An implicit QUICKEST scheme was used to solve the finite difference forms of the momentum equations, and a hybrid scheme of upwind and central differencing was used for the species and energy equations.¹¹ The 50×20 mm computational domain meshed with a 201×81 grid system was clustered to resolve the large gradients in flow variables near the flame zone such that the local grid spacing in the axial and radial directions was 0.2 mm. A nozzle diameter of 5 mm and initial flow velocity of 0.14 m/s was used to match the experimental conditions. A vortex was

issued into the flow by suddenly increasing the nozzle exit velocity to 4.5 m/s with a top-hat velocity profile. Ignition was simultaneously initiated 3 mm above the inflow boundary and 2 mm away from the axis in the radial direction. To simulate secondary instabilities induced by velocity fluctuations, a secondary perturbation was applied to the nozzle exit velocity in the numerical model.

4. Results and Discussion

A series of acetone PLIF images was collected for each of the three piston strokes in order to document the cold-flow conditions. As shown in Fig. 2, the piston stroke has a significant impact on the vortex convection velocity, although the ratio of the vortex core diameter to toroidal ring diameter as a function of distance from the nozzle exit remains fairly constant. This confirms that vortex circulation should be approximately proportional to the vortex convection velocity and, thus, piston stroke.⁴ Note that the nozzle exit is aligned with the bottom of each image and that the red dot near the bottom marks the location of one of the electrodes.

The effect of spark timing is presented in Fig. 3, which shows a sequence of OH PLIF images for each of the spark timings listed in Table 1. The vortex propagation prior to ignition is shown in Fig. 2b, with an equivalence ratio of 1.0 and piston stroke of 3.3 mm. For a spark timing of 2.5 ms, ignition is initiated just ahead of the approaching vortex. The flame propagates quickly into the vortex rollers and remains on the exterior of the jet column where fluid velocity is low. The vortex continues to stretch the flame ahead of the vortex between 4.5 and 7.5 ms and quenches the flame between 7.5 and 8.5 ms. For a spark timing of 4 ms, ignition is initiated as the tip of the vortex passes the electrodes. Vortex-flame propagation is similar to that of the previous case, and a clear annular extinction of flame is shown at 8 ms. This type of extinction is also observed under certain conditions when a vortex of cold fuel impinges on flat counter-flow diffusion flames.¹² For a spark timing of 6 ms, the vortex is beyond the formation stage, and the flame propagates within the jet column and into the vortex rollers. Interestingly, the flame does not propagate down into a second approaching vortex, but remains on the exterior. For a spark timing of 8 ms, the vortex is 4-5 diameters downstream of the electrodes and is unable to propagate into the rollers.

Simultaneous acetone/OH PLIF images are shown in Fig. 4, which allows one to observe the burned and unburned regions simultaneously. The color scaling is adjusted to give contrast between the two signals, with OH PLIF regions appearing red. The images in Fig. 4a correspond to the sequence in Fig. 3b and show the fate of the vortex after the flame is quenched at 8 ms. Note that secondary vortices lead to flame bridging across the jet column and the formation of an island of unburned fuel and air. The images of Fig. 4b show the distortion of the vortex caused by flame propagation.

The effect of equivalence ratio is shown in Fig. 5. The spark timing is at 4 ms after piston actuation and the piston stroke is 3.3 mm. Unlike the stoichiometric conditions shown in Fig. 3b, the lean and rich flames are almost immediately quenched after initial flame formation ahead of the vortex. Flame propagation along the exterior of the jet column is quite similar for equivalence ratios of 0.75 and 1.25 (Figs. 5a and 5b, respectively), but is greatly diminished for an equivalence ratio of 1.5 (Fig. 5c), as expected. Flame bridging, as described previously, occurs across the jet column in Figs. 5a and 5b, but is suppressed in Fig. 5c.

To study the effects of vortex strength on vortex ignition and flame propagation, the ignition timing relative to vortex location was matched for the case shown previously in Fig. 3a (piston

stroke of 3.3 mm) and that of Fig. 6a (piston stroke of 1.6 mm). This can be verified by comparing Fig. 2a at 4 ms and Fig. 2b at 3 ms. Flame propagation is similar for both cases, but the weaker vortex of Fig. 6a does not penetrate the flame ahead of it. The same vortex of Fig. 6a, which is ignited just prior to reaching the electrodes, is ignited just past the electrodes in Fig. 6b. The resulting flame propagates within the jet column and into the vortex rollers, underscoring the need to match ignition timing to the correct phase of vortex development. The conditions for Fig. 7 (piston stroke of 5 mm) were selected such that ignition took place in a similar phase of vortex development as Fig. 3c (piston stroke of 3.3 mm). Again, this can be verified by comparing Fig. 2b at 6 ms and Fig. 2c at 4 ms. For the stronger vortex of Fig. 7, the flame propagates within the jet column and into the vortex rollers much more quickly than in Fig. 3c. In addition, the initial flame lift-off is more dramatic for the stronger vortex of Fig. 7, and local flame perturbations become more apparent. For a spark timing 1 ms later than that of Fig. 7 (see Fig. 2c at 6ms), the flame burns within the jet column but is unable to reach the vortex.

The conditions of the computational model were chosen to simulate flame propagation in the weaker vortex of Fig. 6a. The numerical configuration differs somewhat from experimental conditions because of the asymmetric nature of the ignition process. The presence of a boundary layer at the nozzle exit, uncertainty in the nozzle exit velocity, and nozzle exit velocity fluctuations may also lead to differences in the numerical and experimental results. Nonetheless, the results of the model, shown in Fig. 8, are quite promising. Differences in the selected timing are due to the 0.4 ms time step of the computations. The model predicts flame propagation ahead of the vortex and in the wake region and correctly predicts flame bridging across the jet column. As expected, flame bridging does not take place when the secondary perturbation in the exit velocity is removed.

5. Conclusions

The current study explored several important parameters that affect flame propagation in ignited vortex rings. Flame propagation was found to be highly sensitive to spark timing and was found to take place in two distinct regions: (A) within the jet column and vortex rollers, and (B) on the vortex exterior. Ignition after the passage of a vortex led to Type A flame propagation, and ignition ahead of a vortex led to Type B flame propagation. The equivalence ratio affects the stability and speed of flame propagation, with ideal conditions found at stoichiometric to slightly rich conditions. Higher vortex strength correlated with a higher likelihood of flame extinction for Type A flame propagation, and with faster, more highly wrinkled flame layers for Type B flame propagation. Preliminary results from the numerical model were promising, given uncertainties in boundary and ignition conditions. Future work will focus on obtaining particle image velocimetry data to aid in the computations, as well as more quantitative analysis of product formation.

Acknowledgments

The authors wish to thank Dr. C. D. Carter for his advice in setting up the OH PLIF experiments. The authors also acknowledge the assistance of Dr. R. D. Hancock and Mr. I. Vihinen in the assembly and construction of the burner. This work is supported by U. S. Air Force Contract F33615-00-C-2068.

References

1. Renard, P. H., Thevenin, D., Rolon, J. C. and Candel, S. (2000), "Dynamics of flame/vortex interactions," *Progress in Energy and Combustion Science*, Vol. 26, pp. 225-282.
2. McCormack, P. D. (1971), "Combustible Vortex Rings," *Proceedings of the Royal Irish Academy*, Vol. 71, pp. 73-83.
3. McCormack, P. D., Scheller, K., Muller, G. and Tisher, R. (1972), "Flame propagation in a vortex core," *Combustion and Flame*, Vol. 19, pp. 297-303.
4. Ishizuka, S., Takahiro, M., Takahashi, H., Kiminori, K. and Ryo, H. (1997), "Flame Speeds in Combustible Vortex Rings," *Combustion and Flame*, Vol. 113, pp. 542-553.
5. Cattolica, R. J. (1986), "Combustion-Torch Ignition: Fluorescence Imaging of NO₂," Twenty-First Symposium (International) on Combustion, The Combustion Institute, pp. 1551-1559.
6. Cattolica, R. J. and Vosen, S. R. (1986), "Two-Dimensional Fluorescence Imaging of a Flame-Vortex Interaction," *Combustion Science and Technology*, Vol. 48, pp. 77-87.
7. Wilson, K. J., Gutmark, E., Yu, K. H. and Schadow, K. C. (1994), "Active Control of Bluff-Body Flame Holder Combustor," AIAA Paper No. 940215, 32nd Aerospace Sciences Meeting & Exhibit, Reno, NV.
8. Rolon, J. C., Aguerre, F. and Candel, S. (1995), *Combustion and Flame*, Vol. 100, pp. 422-429.
9. Fiechtner, G. J., Renard, P. H., Carter, C. D., Gord, J. R. and Rolon, J. C. (2000), "Injection of Single and Multiple Vortices in an Opposed-Jet Burner," *Journal of Visualization*, Vol. 2, pp. 331-341.
10. Katta, V. R., Goss, L. P. and Roquemore, W. M. (1994), "Effect of non-unity Lewis number and finite-rate chemistry on the dynamics of a hydrogen-air jet diffusion flame," *Combustion and Flame*, Vol. 96, pp. 60-74.
11. Katta, V. R., Goss, L. P. and Roquemore, W. M. (1994), "Numerical Investigations of Transitional H₂/N₂ Jet Diffusion Flames," *AIAA Journal*, Vol. 32, pp. 84-94.
12. Katta, V. R., Carter, C. D., Fiechtner, G. J., Roquemore, W. M., Gord, J. R. and Rolon, J. C. (1998), "Interaction of a Vortex with a Flat Flame Formed Between Opposing Jets of Hydrogen and Air," Twenty-Seventh Symposium (International) on Combustion, The Combustion Institute, pp. 587-594.

Table 1. Experimental Conditions.

Ignition Timing (ms)*	Equivalence Ratio	Piston Stroke (mm)	Vortex Velocity (m/s)
2.5	1.0	3.3	5
4	0.75, 1.0, 1.25, 1.5	3.3	5
4	1.0	1.6	2.5
5	1.0	5	6.5
6	1.0	1.6, 3.3, 5	2.5, 5, 6.5
8	1.0	3.3	5

* Relative to piston actuation

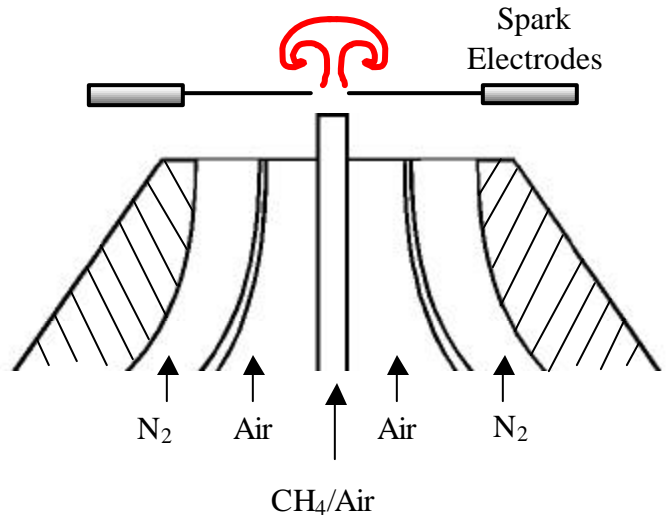
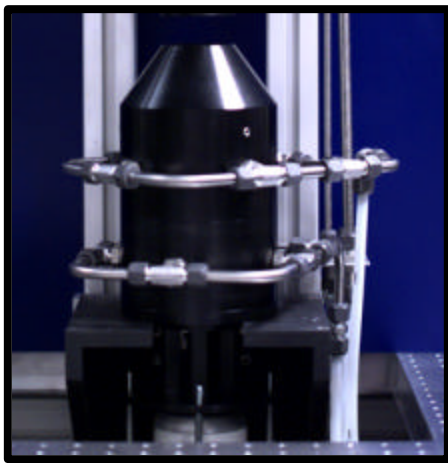


Fig. 1. Jet-in-co-flow burner used for vortex ignition experiments

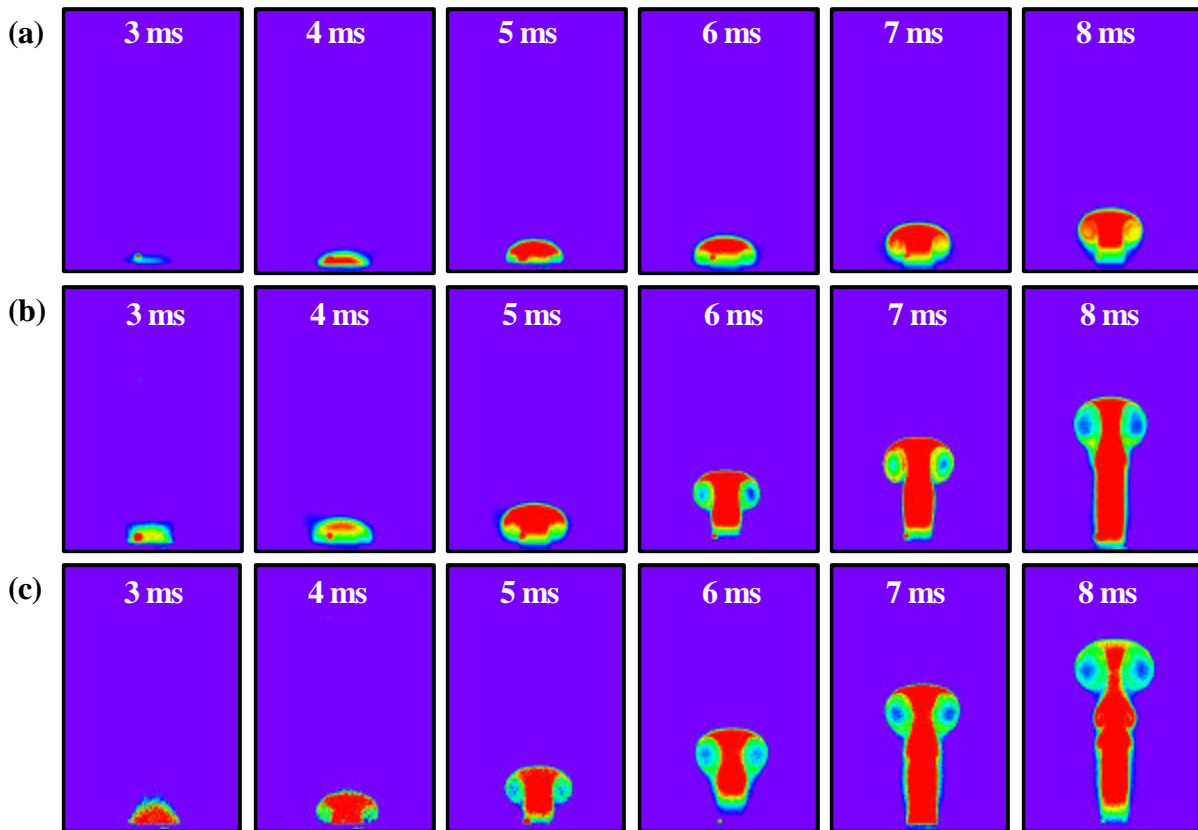


Fig. 2. Acetone PLIF images of cold-flow vortex propagation as a function of time after the piston is actuated for piston strokes of (a) 1.6 mm, (b) 3.3 mm, and (c) 5 mm.

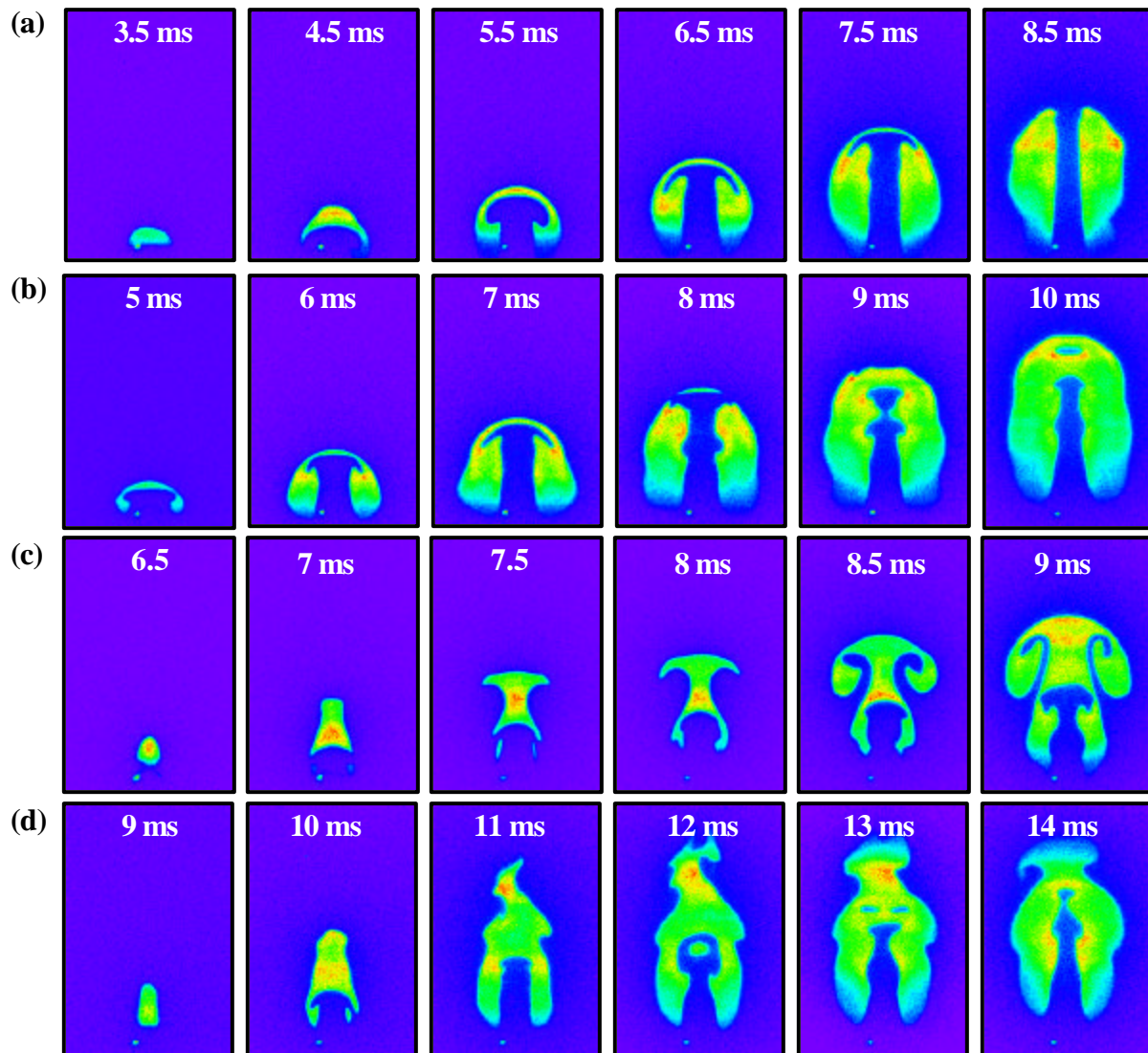


Fig. 3. OH PLIF image sequence for spark timings of (a) 2.5 ms, (b) 4 ms, (c) 6 ms, and (d) 8 ms after piston actuation. Equivalence ratio is 1.0 and piston stroke is 3.3 mm.

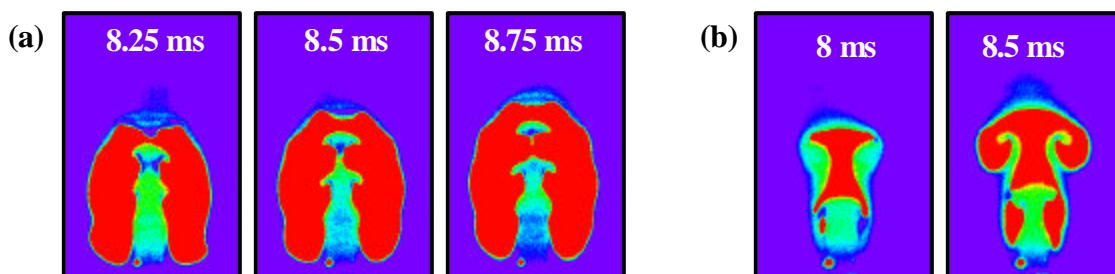


Fig. 4. Partial sequence of Acetone/OH PLIF images for spark timings of (a) 4 ms and (b) 6 ms after piston actuation. Equivalence ratio is ~ 1.0 and piston stroke is 3.3 mm. Images scaled such that regions of OH appear red.

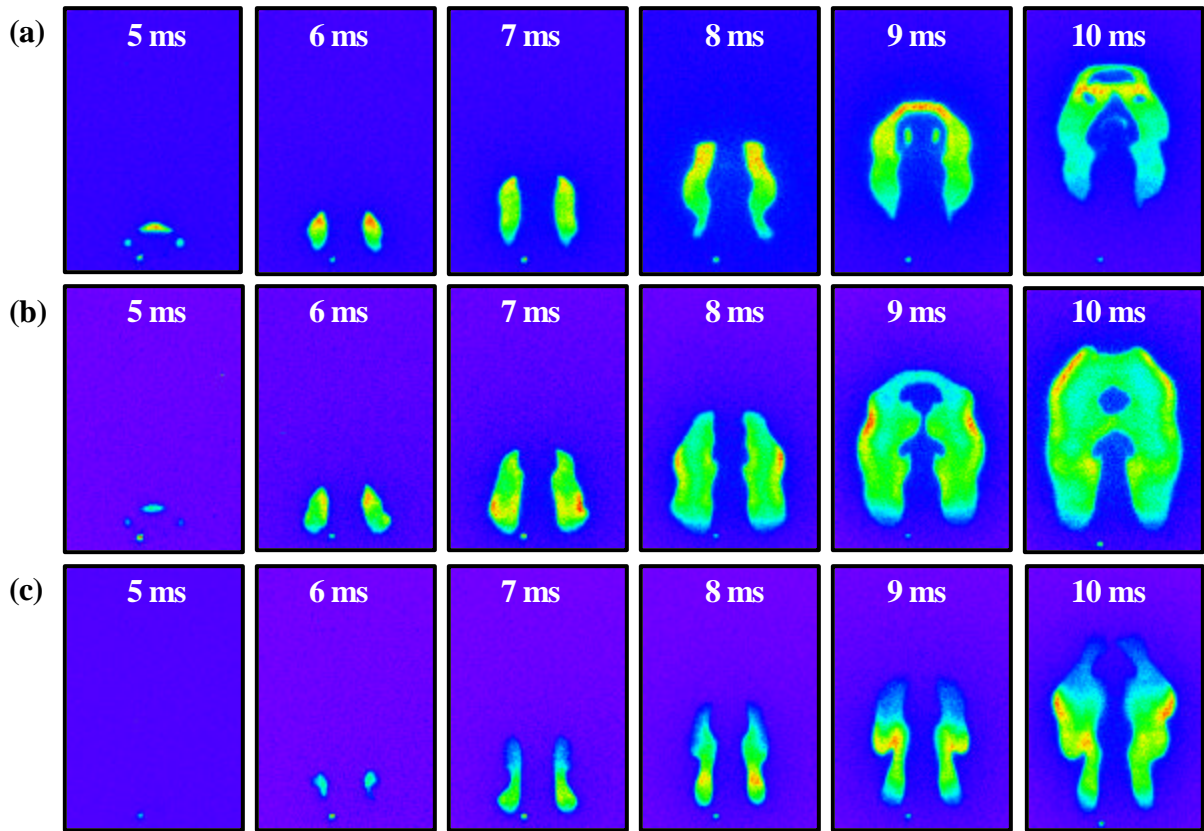


Fig. 5. OH PLIF image sequence for equivalence ratios of (a) 0.75, (b) 1.25, and (c) 1.5. Spark timing is 4 ms after piston actuation and piston stroke of 3.3 mm.

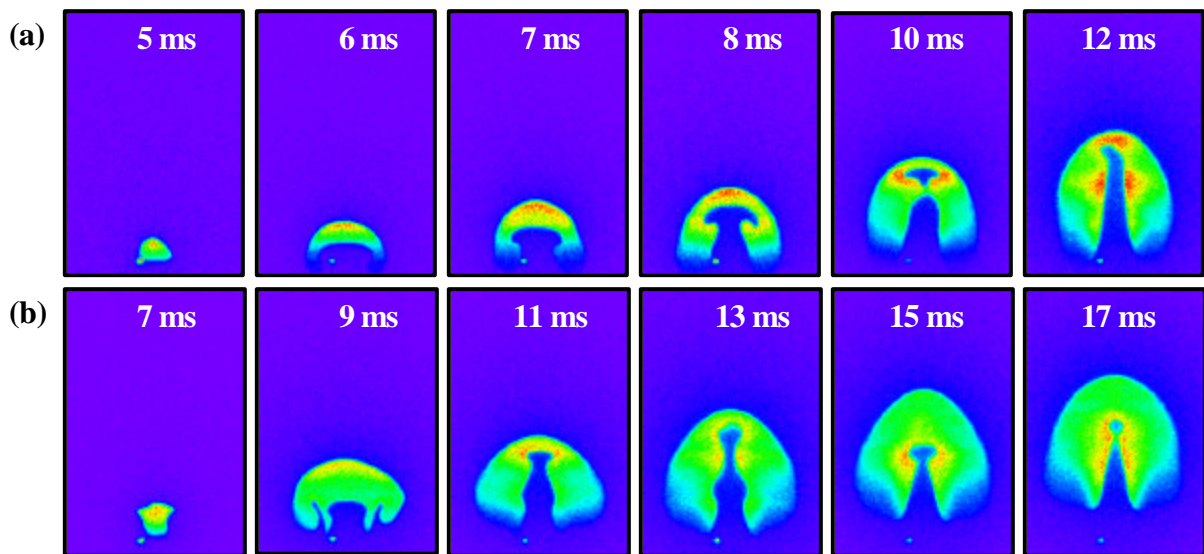


Fig. 6. OH PLIF image sequence for a piston stroke of 1.6 mm and spark timings of (a) 4 ms and (b) 6 ms after piston actuation. Equivalence ratio is 1.0.

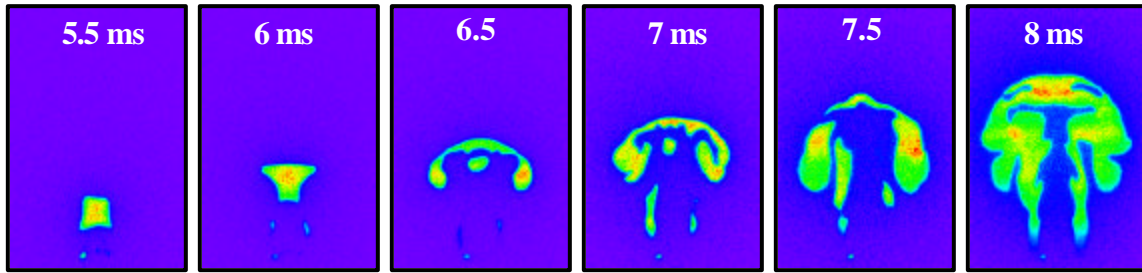


Fig. 7. OH PLIF image sequence for a piston stroke of 5 mm and spark timing of 6 ms for comparison with Fig. 3c. Equivalence ratio is 1.0.

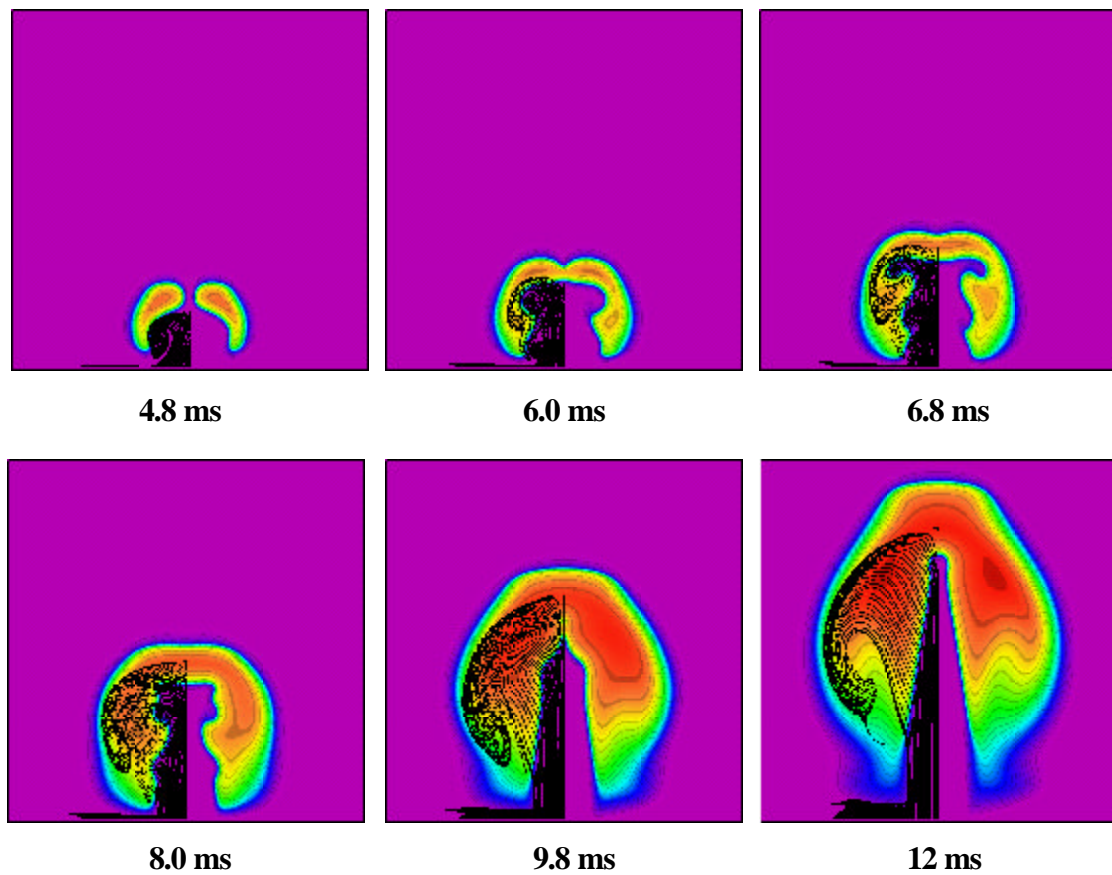


Fig. 8. Computed temperatures and particle traces simulating a 1.6 mm piston stroke. Ignition is initiated as the vortex exits the nozzle at ~ 4.0 ms. Image width and height are 20 mm.